A PHOTOMETRIC STUDY OF THE YOUNG STELLAR POPULATION THROUGHOUT THE λ ORIONIS STAR-FORMING REGION

CHRISTOPHER J. DOLAN[1,2] AND ROBERT D. MATHIEU[1]

ABSTRACT

We present *VRI* photometry of 320,917 stars with $11 \lesssim R \lesssim 18$ throughout the λ Ori star-forming region. Using the more spatially limited spectroscopic surveys of Dolan & Mathieu to define the color-magnitude domain of young low-mass members of the association and removing statistically the field stars in this domain, we use our photometry to identify a representative pre–main-sequence (PMS) population throughout the interior of the molecular ring. The spatial distribution of this population shows a concentration of PMS stars around λ Ori and in front of the B35 dark cloud. However, few PMS stars are found outside these pockets of high stellar density, suggesting that star formation was concentrated in an elongated cloud extending from B35 through λ Ori to the B30 cloud. We find a lower limit for the global stellar mass of about 500 $M_\odot$. We find that the global ratio of low- to high-mass stars is similar to that predicted by the field initial mass function, but this ratio varies strongly as a function of position in the star-forming region. Locally, the star formation process does not produce a universal initial mass function. Using our derived stellar ages across the region, we construct a history of the star-forming complex. This history incorporates a recent supernova to explain the distribution of stars and gas today. We infer that most of the present molecular ring was formed by ejecta from the center driven by the supernova blast about 1 Myr ago. However, we suggest that the B30 and B35 clouds were primordial, and massive enough to be mostly little disturbed by the shock. The stars that we see today trace the former extent of the cloud complex. Given the kinematics of the stellar population, we predict that the association will disperse into the field within a few tens of megayears.

Key words: stars: formation — stars: pre–main-sequence

On-line material: machine-readable tables

1. INTRODUCTION

Much of our understanding of the process of low-mass star formation arises from studies of individual young stars. Historically, the most popular regions for the study of these stars are nearby dark clouds, such as Taurus-Auriga, Chaemeleon, Lupus, and ρ Oph. In these regions, the T Tauri stars interact with the local interstellar medium with parsec-long jets and substantial molecular outflows, but their spheres of influence are usually smaller than their separations. Thus models of star formation that arise from observations of stars in such T associations often consider only stars in isolation.

Recent advances in technology have permitted detailed studies of low-mass stellar populations in OB associations. The most massive members of such OB associations have large spheres of influence and may assail the entire star-forming region with dissociating or ionizing radiation or disrupting winds. Thus the massive stars must be integrated into the formation process of associated low-mass stars.

Can the massive stars terminate nearby star formation by destroying the gas clouds? Alternatively, can they enhance star formation by compressing the clouds? Could both of these effects occur in different regions of the same star-form-ing complex? Can these effects change the resulting spatial and mass distributions of young stars?

Recent studies are beginning to answer all of these questions affirmatively. In cases where the massive stars ionize clouds and reveal embedded stars (e.g., Eagle Nebula; Hester et al. 1996) or evaporate circumstellar disks of existing stars (e.g., Trapezium, Bally et al. 1998), it is clear that massive stars have *terminated* star formation. On the other hand, Walter et al. (1994) and Preibisch & Zinnecker (1999) show that star formation in the Upper Scorpius OB association was likely *triggered* by a nearby supernova, since all the stars were formed within a very short time span.

For many years, star formation was hypothesized to be bimodal: low-mass and high-mass stars were thought to form under very different conditions (see Shu & Lizano 1988). With the notable exception of the Trapezium, evidence for low-mass stars near OB stars was lacking until the 1980s. Since then, however, young low-mass stars have been shown to be ubiquitous. In particular the *ROSAT* All-Sky Survey found young, low-mass stars associated with OB stars throughout the Gould Belt (Guillout et al. 1998). Since this realization, surveys have demonstrated that the initial mass functions (IMFs) of several OB associations are consistent with the field IMF (e.g., Preibisch & Zinnecker 1999 in Upper Sco; Hillenbrand 1997 in the Trapezium). But these statements are for the global IMF of the star formation regions. In many associations, the OB stars are more spatially concentrated than the rest of the stars. Except perhaps in very high density environments such as the Trapezium, these associations are too young for dynamical mass segregation. Perhaps some aspect of the star-forming

---

[1] Department of Astronomy, University of Wisconsin–Madison, 475 North Charter Street, Madison, WI 53706; mathieu@astro.wisc.edu.

[2] Visiting Astronomer, Kitt Peak National Observatory (KPNO), National Optical Astronomy Observatory, which is operated by the Association of Universities for Research in Astronomy, Inc., under cooperative agreement with the National Science Foundation.

process skews the local IMF toward high-mass stars in some locations and low-mass stars in others.

To make a comprehensive exploration of the effect of massive stars on low-mass star formation, this paper employs a photometric survey for young low-mass stars throughout the λ Orionis OB association. The λ Ori region is a superb laboratory for studying the evolution of a molecular cloud into an association of low- and high-mass stars. The star-forming complex contains a tight knot of OB stars encircled by a 40 pc diameter ring of dense molecular gas and dust (see Fig. 15 of Dolan & Mathieu 2000). Notable features of this clumpy ring include the large B30 cloud on the northwest edge and the elongated B35 cloud protruding inward from the eastern side. By contrast, the interior of this ring is nearly devoid of dense gas. It is this relative transparency that has made the λ Ori region both understudied in the past and appealing for the present study of the young stellar population: the lack of opacity reveals the entire member population, as well as vast numbers of background field stars. Until recently, comprehensive studies have been heavily biased toward stars with strong emission features, such as Hα (Duerr, Imhoff, & Lada 1982) or X-rays (Sterzik et al. 1995 and several subsequent works).

In Dolan & Mathieu (1999, hereafter Paper I) and Dolan & Mathieu (2000, hereafter Paper II), we studied a spatial subset of the λ Ori region, focusing on a 6°-long region extending from B30 to B35 through the central concentration of OB stars. For nearly every star in that region with $12 < R < 16$ and redder than a 30 Myr D'Antona & Mazzitelli (1994) isochrone (3618 stars), we obtained a high-resolution spectrum with the WIYN[3] Multi-Object Spectrograph (MOS). From these, we identified 266 pre–main-sequence (PMS) stars via the presence of strong lithium λ6708 absorption, a secure diagnostic of youth. Using model evolution tracks to determine ages, we found that low-mass star formation started simultaneously with the OB stars 6–8 Myr ago and has accelerated since then. However, we found a marked difference in recent star formation rates at different locations: within 2° of the OB stars there are almost no stars younger than 1 Myr, while farther away stars of this young age are plentiful. These differing age distributions led to our conclusion that there was a supernova 1 Myr ago, which disrupted further star birth in the vicinity of the OB stars. The model evolution tracks also yielded masses for the PMS stars. Compared with the massive OB stars, we concluded that globally the IMF of the λ Ori star-forming region was consistent with the field IMF, but there were significant local variations: the high-mass stars dominated the central region while low-mass stars dominated at larger radii. Those low-mass stars closest to the OB concentration also show a remarkable lack of Hα emission at all ages. We attributed this to FUV radiation from the massive stars destroying the circumstellar disks of those stars.

The age and mass data for the PMS stars showed us that nearly all of the detected PMS stars lie in a region of the $R-I$ versus R color-magnitude diagram brighter and redder than the bulk of the field stars. This result suggested that photometric analysis would be an effective tool for identifying and removing well over 99% of the field stars. To exploit

this feature, we have imaged most of the λ Ori region in VRI and produced a comprehensive stellar photometric database. With these data, we identify all stars in the region of the CMD where PMS members of the association are likely to lie. Using the subset of fields where we have spectroscopic data (Paper II), we construct a model of the field star distribution. Statistically removing the field stars, we are left with a stellar sample representative of the true PMS population.

This representative sample allows us to examine the spatial distribution of the young population. This sample also permits us to count the total number of low-mass members and thereby compare the association IMF with the field IMF. In combination with the high- and low-mass stellar age distribution derived in Paper II, we develop in this paper a comprehensive history of star formation in the λ Ori association.

2. DATA

In § 2 of Paper II we presented a summary of our broadband photometric survey of the λ Ori region. This paper presents a more detailed description and analysis of those photometric data. Unlike Paper II, we discuss only the "1999 photometry" in the following. In fact, some stars with older photometry from 1997 and 1998 are included in the data set presented here, where we have rare, accidental holes in our 1999 sky coverage, but this accounts for just 0.1% (361 of 320,917) of the stars, so we ignore those older data sets in the following discussion.

2.1. *Acquisition*

During 1999 December 15–20 we used the Mosaic imager on the KPNO 0.9 m telescope to survey about 60 degrees² of the λ Ori star-forming region in VRI. This region includes the central concentration of OB stars, portions of the encircling ring of molecular clouds, and the nearly gas-free region in between.

The Mosaic imager is highly effective for such a survey with its nearly 1° field of view and pixel size of 0″.42. In total, we observed 61 fields with VRI filters. Table 1 summarizes the conditions of the observing run. A more detailed analysis of individual fields from each night is included in § 2.3. In general, the run was of high quality, but thin clouds affected a few fields, as described below. The full moon was very close to the star-forming region on the last nights, causing the signal-to-noise ratio (S/N) for stars of a given magnitude to be lower.

Prior to the run, we had selected 83 fields to observe, but anticipating that weather would prevent us from finishing all of these, we observed the fields in a priority order based

---

[3] The WIYN Observatory is a joint facility of the University of Wisconsin-Madison, Indiana University, Yale University, and the National Optical Astronomy Observatory.

TABLE 1
OBSERVING SUMMARY

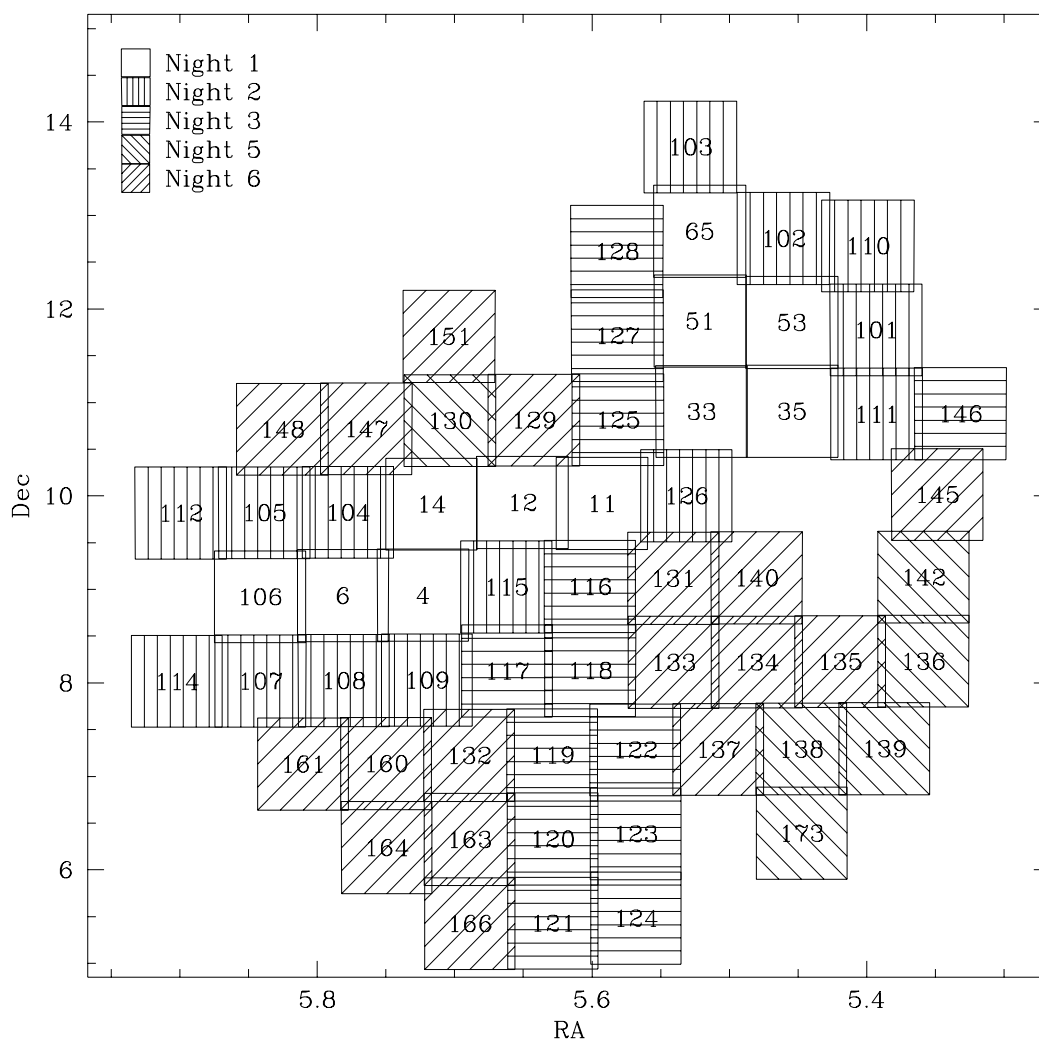| Night	Date	Fields VRI	Comments
1.........	Dec 15	11	Very good, then cirrus just before dawn
2.........	Dec 16	14	Cirrus at dusk, then very good
3.........	Dec 17	13	Perfect
4.........	Dec 18	0	Thick clouds, no data
5.........	Dec 19	6	Cirrus early, then clear with bright moon
6.........	Dec 20	17	Full moon, no clouds

Fig. 1.—Map of the *VRI* KPNO Mosaic fields observed in 1999 December (with internal identification numbers). The fields are shaded according to the night on which they were observed.

on the following criteria: fields which had been observed in 1997 and 1998 (to provide improved photometry for those crucial regions), fields adjacent to and overlapping the 1997 and 1998 fields, fields which overlapped archival *ROSAT* pointings (for future comparisons with the X-ray data), and regions which appeared interesting in the Lang & Masheder (1998) CO map (particularly, the B223 cloud and the small, elongated cloud south of B35).

Figure 1 shows the location of the observed *VRI* fields. The field numbers marked on Figure 1 indicate our priority order in the sense that a lower number is higher priority. Table 2 presents a cross-reference to the field names used in Paper II. We present the center coordinates for these fields as observed in Table 3, as well as the night on which the field was observed (cross-referenced to Table 1). (For those fields not observed, a 0 is given for night observed and the intended field center is provided for possible future extension of the survey.) Due to problems with telescope pointing, the actual field centers are often $15''$–$20''$ (and up to $1.'3$ for some fields on night 1) away from the intended coordinates. Since we usually overlapped adjacent fields by $5'$, this is typically not a problem in terms of areal coverage.

For each observed field, we took three exposures per filter, each shifted 100 pixels (about $43''$) in right ascension

and declination. This is the minimum number needed to cover the inter-CCD gaps in the Mosaic imager. For almost 97% of the image, where there are no gaps or bad pixels, the multiple exposures increase the signal by three when combined. For just over 3% of the field, a star will lie on a gap in one of the three exposures. Our photometry of such a star would only use signal from the other two, which corresponds to a 19% S/N degradation relative to the regions with full coverage. Finally, 0.1% of the field lies on the intersection of gaps from two images, which translates to a 43% lower S/N than when all three images can be used.

TABLE 2
FIELD NAME CROSS REFERENCE

Paper II	This Paper	Paper II	This Paper
1..............	107	7................	33
2..............	4 and 6	8................	35
3..............	4	9................	51
4..............	14	10..............	53
5..............	12	11..............	65
6..............	11		

Field	R.A.	Decl.	Night
4.........	05 43 23.01	08 56 20.93	1
6.........	05 46 53.02	08 56 03.43	1
11.......	05 35 33.56	09 55 13.14	1
12.......	05 39 02.40	09 55 50.89	1
14.......	05 43 00.89	09 54 46.50	1

NOTES.—Table 3 is presented in its entirety in the electronic edition of the Astronomical Journal. A portion is shown here for guidance regarding its form and content. Units of right ascension are hours, minutes, and seconds, and units of declination are degrees, arcminutes, and arcseconds (equinox 2000.0). The final number is the night observed, cross-referenced to Table 1. Fields with a 0 were not observed, and the intended field centers are provided.

For each exposure, we used the following exposure times: 18 s in I, 15 s in R, 27 s in V. These times were chosen to yield an S/N better than 100 in VRI in the co-added images for a star with $R = 16$ and $V−R = 1$, while preventing $R = 12$ stars from saturating.

For photometric calibration, each night we took single VRI exposures of seven to 10 fields containing Landolt (1992) standard stars. We achieved nearly uniform sampling in air mass from at least 1.2 to 2.0 each night. We always observed one or more of these calibration fields before the first and after the last science field of each night.

We also obtained 10 bias exposures, five dome flats, and a few twilight flats per filter each night. Over the course of the six nights, we gathered enough twilight flats to make one high-S/N flat in each filter. We discuss the relative merits of dome and twilight flats in the next section.

2.2. Reduction

We reduced all of our images with IRAF-MSCRED V3.2.3, closely following the data reduction guide written for V2.0 by F. Valdes. First, for each night we combined the bias images into a single image. It is clear from these images that the bias voltages for the Mosaic CCDs are unstable at the 2–3 ADU level over a timescale of minutes, so for all subsequent images we subtracted both the overscan strip and the combined bias image for the appropriate night.

Also, for each night we combined the dome flats for each filter into a single image. Dividing dome flats from different nights as a test, we immediately noticed substantial deviations from unity, often in the form of strong gradients. Communication with G. Jacoby led us to believe that this may have arisen because we were insufficiently careful when pointing the telescope at the dome white spot when taking these flats. The small spot compared with the wide field of the camera requires pointing to within $1'$ to prevent large vignetting. This problem led us to reject the dome flats.

Instead, we used the twilight flats for flat fielding. First we selected the twilight flats from each night with mean count levels of 7000–15,000 ADU (nine in I, 10 in R, and 15 in V). We combined these to create one combined flat per filter for the entire run. Contrary to typical techniques, we did not preflatten these with the dome flats.

We performed initial image reductions on the Landolt fields with MSCRED-CCDPROC using the twilight flats.

For each field we then found a single star from the Tycho catalog (ESA 1997) with $V \sim 12$ to roughly register the VRI images using MSCZERO. We computed more detailed astrometry for each image with MSCCMATCH using 500–1000 stars from the USNO-A2.0 catalog (Monet et al. 1996) with $11 < R \lesssim 14.5$. This typically yielded astrometric solutions with rms errors of $0\rlap{.}''7$ to $0\rlap{.}''9$ in right ascension and $0\rlap{.}''5$ to $0\rlap{.}''8$ in declination. Using these solutions, we resampled the images to the sky tangent plane with MSCIMAGE. This latter step was essential to correct the nonuniform plate scale caused by the field corrector on the telescope. Additionally, we found that redoing the astrometric solution with CCMAP after resampling allows us to improve the rms coordinate residuals to about $0\rlap{.}''6$ in right ascension and $0\rlap{.}''45$ in declination. The greatest improvements occur at the edges and corners of the image, where the position implied by the coordinates may move by up to a pixel or two. We see this improvement because CCMAP is more flexible than MSCCMATCH, and it appears that there are minor imperfections in the NOAO-provided plate solution for the Mosaic field.

Finally, using the reduced Landolt field images, we manually identified and centroided each Landolt star with IMEXAMINE and ran PHOT on those stars. We used the relative magnitudes reported by PHOT to test the photometricity of each night. With one small exception, we found that nights 1–3, 5, and 6 are all of high quality, with rms fit residuals of 0.030 (B), 0.027 (V), 0.027 (R), and 0.029 (I) mag. The one exception is the last hour of night 1, when thin clouds appeared unexpectedly. These clouds ruined the last Landolt field and damaged the three previous science fields. The repair of these three fields is described below in § 2.3. As significant difference in the photometric parameters were not found between the nights, we combined the observations of standards on all photometric nights to compute the CCD and atmospheric parameters for the run. To accomplish the latter, we used FITPARAMS for each filter to solve for four coefficients: the zero-point, color, air-mass, and color–air-mass terms.

The initial stages of the reduction of the VRI science fields were identical to those of the Landolt fields. However, we employed the additional step of combining the three exposures per filter for the survey fields. After resampling the images to the sky tangent plane, we median-combined the multiple exposures with MSCSTACK to make a single image. Because the MSCIMAGE task allows one to register images while resampling, there was no need for a separate registration step.

Next, we identified the targets for which we wish to compute photometry. Rather than attempting to identify sources in our images with a tool like DAOFIND, we have adopted the point-source detections from the USNO catalog. This choice has both positive and negative consequences. The main advantage is that we can trust that our targets are genuine stars and not extended sources, cosmic rays, or CCD artifacts. In addition, we do not have to attempt the difficult task of cross-referencing our target detections from the different filters: we use the same target list for all filters. The main disadvantage is that the Palomar survey, on which the USNO catalog is based, has slightly coarser resolution than the Mosaic, so a close pair that is resolvable in our field could appear blended as a single star in the USNO catalog. Another potential problem is that the USNO coordinates are epoch 1950–1956 and so may be inaccurate for epoch

1999. This concern is minimized because (1) λ Ori is very near the anticenter of the solar motion so solar reflex motion is small; (2) we suspect relative proper motions of member stars of the association are quite low, as they are in the Orion Nebula Cluster (most recently measured as $\mu \simeq 0.08$ mas yr^{-1}; Tian et al. 1996); and (3) we are using large apertures. Using the astrometric solution from CCMAP above, we transform the right ascension and declination coordinates into pixel coordinates for all USNO-A2.0 stars with $R < 18$.

We then performed aperture photometry with PHOT on the USNO positions. Because the λ Ori region is not crowded, we used a generous aperture radius of 12 pixels (about 5″), as we did for the Landolt stars. For background subtraction, we used a sky annulus with inner and outer radius of 18 and 27 pixels, respectively. Following the PHOT task, we used the VRI portion of the Landolt solution with the INVERT task to compute calibrated magnitudes for each star. After removing the invalid stars (ones flagged by IRAF as saturated or on the edge of the image), this resulted in photometry of 3000–9000 stars per field (varying primarily as a function of Galactic latitude and cloud density in the star-forming complex).

In Table 4 we present V, R and I photometry for all stars, sorted by right ascension. Where we have multiple measurements, we average the V, R, and I quantities. The quoted errors, derived in the following section, are separated into the three domains, where we are limited by systematics ($12 < R < 16$), photon noise ($16 < R < 17$), and sky background ($17 < R < 18$). The final three columns contain J2000.0 coordinates from the USNO-A2.0 catalog and the field(s) in which the star was observed.

Figure 2 shows the position of all survey stars with $11.5 < R < 16.5$. With these 138,576 stars marked as black dots, regions of high extinction show up clearly in white, signifying an absence of background stars. These regions closely correlate with the $IRAS$ infrared image of the dense molecular clouds shown in Figure 16 of Paper II. Thus Figure 2 vividly demonstrates that most of the stars in the data set are background stars.

2.3. *Photometric Quality*

With three exposures per field and overlapping regions between fields, we have many opportunities for internal quality checks. Paper II discussed in detail the quality of a subset of the photometry, primarily from nights 1 and 2. Here we discuss the entire data set, first in a global sense and then followed by an investigation into differences between fields.

In Paper II we evaluated our internal errors based on comparisons of photometry derived from each of the three exposures for each field and filter. There, we found an internal limiting precision of 0.016 mag in all bands for bright stars ($R < 15.5$). For single exposures, stars with $15.5 < R < 17$ are photon limited, while stars fainter than $R = 17$ are limited by sky brightness. These limits can be seen in the top panel of Figure 3, which shows the measured magnitude differences derived from any two of the three R exposures of field 110. However, as we will show below, external systematic effects dominate stars brighter than $R = 16$, so the 0.016 mag precision is not achieved.

Our external errors can be assessed by comparison of photometric measurements of any star observed more than once. Such multiple observation come from fields which overlap each other on edges or corners, totaling to 44,414, 3052, and 399 stars with two, three, or four observations, respectively. For these stars we computed standard deviations of R magnitude measurements. To study the distribution of standard deviations, we divided the stars into six bins according to their mean R magnitude. Inverse Gaussian analysis of each of the magnitude intervals found the standard deviations of these distributions to be 0.12 ($18 > R > 17$), 0.069 ($17 > R > 16$), 0.047 ($16 > R > 15$), 0.041 ($15 > R > 14$), 0.039 ($14 > R > 13$), and 0.037 ($13 > R > 12$) mag. These numbers demonstrate that photometric quality is only weakly a function of magnitude for stars with $R < 16$. The asymptotic approach to a standard deviation of about 0.030 mag indicates a systematic limit on our photometric precision. For the faintest stars, the photometry deteriorates rapidly as the moonlit sky brightness begins to dominate. Thus we use the dispersions quoted above as our photometric uncertainty in Table 4 for stars fainter than $R = 16$.

However, for stars brighter than $R = 16$ this analysis underestimates the quality of the photometry. We have found that the field-to-field overlap regions at the edges of the images (from where all of our multiple measurements derive) suffer significantly worse photometry than the rest of the images. There are two main systematic effects which degrade the photometric quality. First, when we compare photometry between fields which overlap north-south, we

TABLE 4
VRI PHOTOMETRY

ID[a]	V[b]	R_C[b]	I_C[b]	R.A.	Decl.	Field(s)
lOri J051750.9 + 103824	16.738	15.993	16.838	05 17 50.916	10 38 23.84	146
lOri J051751.2 + 102548	18.714	17.319	16.622	05 17 51.197	10 25 47.72	146
lOri J051751.5 + 105655	15.396	14.862	14.282	05 17 51.502	10 56 55.41	146
lOri J051751.5 + 103716	16.674	15.930	15.304	05 17 51.515	10 37 16.45	146
lOri J051751.6 + 105902	17.676	17.070	16.314	05 17 51.593	10 59 01.69	146

NOTES.—Table 4 is presented in its entirety in the electronic edition of the Astronomical Journal. A portion is shown here for guidance regarding its form and content.

[a] The identifier is constructed from the USNO-A2.0 coordinates. For the 110 stars where this identifier is not unique, we have appended an "a" for the westernmost or a "b" for the easternmost star to distinguish between them.

[b] The mean photometric error is 0.032 ($12 < R < 16$), 0.069 ($16 < R < 17$), or 0.12 ($17 < R < 18$) mag, as described in the text.
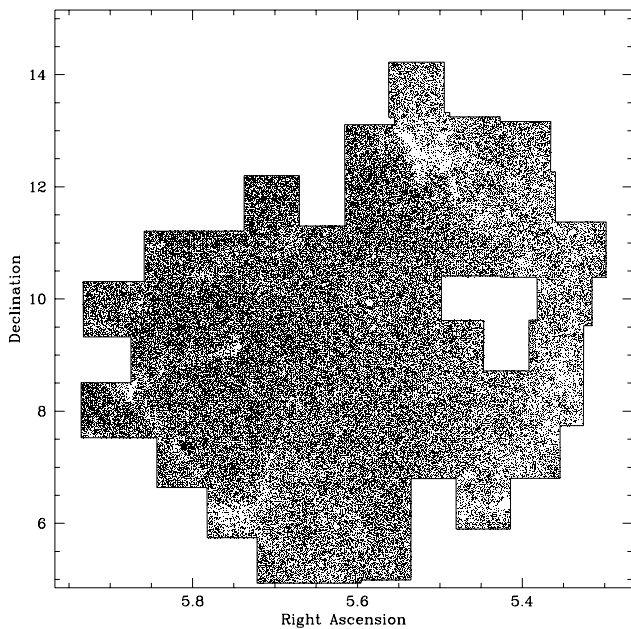
Fig. 2.—Map of all stars with $11.5 < R < 16.5$. Stars are shown as black dots. The white areas show regions of high extinction associated with the ring of molecular clouds around λ Ori.

find that there is a systematic offset. This offset has a mean value of 0.029 (V), 0.047 (R), or 0.051 (I) mag measured from all multiply measured stars with $11 < R < 16$ in the 64 pairs of north-south adjacent fields. These offsets are in the sense that stars at the north edge of the southernmost field appear fainter than the same stars observed in the south edge of the northernmost field. Measuring this magnitude difference as a function of position within the overlapping strip, we find that the most deviant photometry comes from within $\sim 1'$ of the very edge of the chip and improves rapidly toward the interior of the chip. We find the dispersion of magnitude *differences* to be 0.048 mag in all three filters, corresponding to a true measurement precision of a single observation of 0.034 mag.

For the 47 fields that overlap east-west, on the other hand, we find mean offsets near zero in all filters. The single measurement dispersion is 0.030 mag, similar to the difference dispersion found at the north-south edges.

Given the restriction of the north-south photometric offsets to the outer couple arcminutes of the field of view and the uniform photometric quality with position in the east-west overlap regions, we are confident that photometry over almost all of a field is of uniform quality. In the absence of independent photometry, we choose to minimize the impact of the north-south offset by averaging together all multiple measurements. We nonetheless caution that the photometry of stars within a few arcminutes of the north or south boundary of a field is likely less accurate than the rest of the stellar sample.

The second effect that systematically degrades the photometric quality is the proximity of the moon on the later nights of the run. By night 6, the moon was 97% full, and only 18° northwest of λ Ori. These conditions forced us to select targets in the southeast quadrant of the star-forming region until the moon was occulted by the dome in the last third of the night. These conditions inflated the resulting photometric dispersion between overlapping fields by 15% or more for stars with $R > 16$.

To more accurately quantify the effect of the moon, we recomputed the photometric precision excluding all fields from nights 5 and 6, which translates to excluding almost 50% of the multiply measured stars. The offsets (either north-south or east-west) did not change appreciably, but the dispersion of the magnitude differences decreased to 0.030 (north-south) or 0.029 (east-west) mag for a single field. Comparable tests including *just* nights 5 and 6 yield 0.036 and 0.033 mag.

In conclusion, we adopt an intermediate estimate of 0.032 mag for our photometric precision in all filters. The photometry may be worse near the north and south edges of the fields, but those are regions where we have multiple measurements whose combination will reduce the errors. In addition, we warn that this precision varies from field to field. In particular we note that the slightly lower quality photometry from later nights of the run are at systematically larger radii from λ Ori.

Finally, we found a few fields to have anomalous photometry. We observed six instances (fields 109, 110, 112, 128, 138, and 173) where one exposure in one filter had photometry that disagreed with the other two exposures by between 0.02 and 0.10 mag. In one additional case (field 111), one exposure in each of the three filters suffered similar defects. Figure 3 shows data from field 110 as an example comparing the three exposures in a normal filter alongside three exposures from a problematic filter. From this comparison, one can see the obvious 0.030 mag offset in exposure 2 of the I filter. In all cases, the observed discrepancies were in the sense that the anomalous exposure generated fainter magnitudes than the others. We are not certain about the cause of these irregularities. It could be very thin cirrus, which we did not notice at the telescope. Or, perhaps more likely, it could be due to partial occultation by the dome, since we had problems with the dome drive motor overshooting its target azimuth throughout the run. We have responded to these problems in the data with two procedures. For fields 138 and 173, which each had small offsets of about 0.03 mag for one exposure, we simply applied a correction to that one exposure to match the others before the co-adding step. A follow-up comparison with the overlapping neighbors show that this correction was successful. For the rest of the problematic fields, we simply discarded the errant exposure and combined the other two exposures alone. Subsequent checking against the adjacent fields showed that photometry derived from those remaining exposures is of high quality. Discarding one exposure caused us to miss a few stars in the interchip gaps in the affected filter, but the effect is minor.

In addition, we have three fields (fields 4, 6, and 106, observed in this order of time) which were apparently contaminated by unnoticed cirrus at the end of night 1. The gradual arrival of these clouds is obvious when these fields are compared with adjacent fields observed on different nights. The fields surrounding the affected ones all had very high quality photometry, which allowed us to compute precise offsets. The first two filters of field 4 are unaffected while the third (I) suffers 0.015 mag of extinction. Next, field 6 suffers extinction in all three filters of 0.032 (V), 0.053 (R), and 0.044 (I) mag. Finally, field 106 suffers 0.092 (V), 0.144 (R), and 0.299 (I) mag of extinction. We used these measured offsets as corrections, which we applied to the final photometry for each of these fields. Since the corrections are small (at least for fields 4 and 6), the errors in the color correction
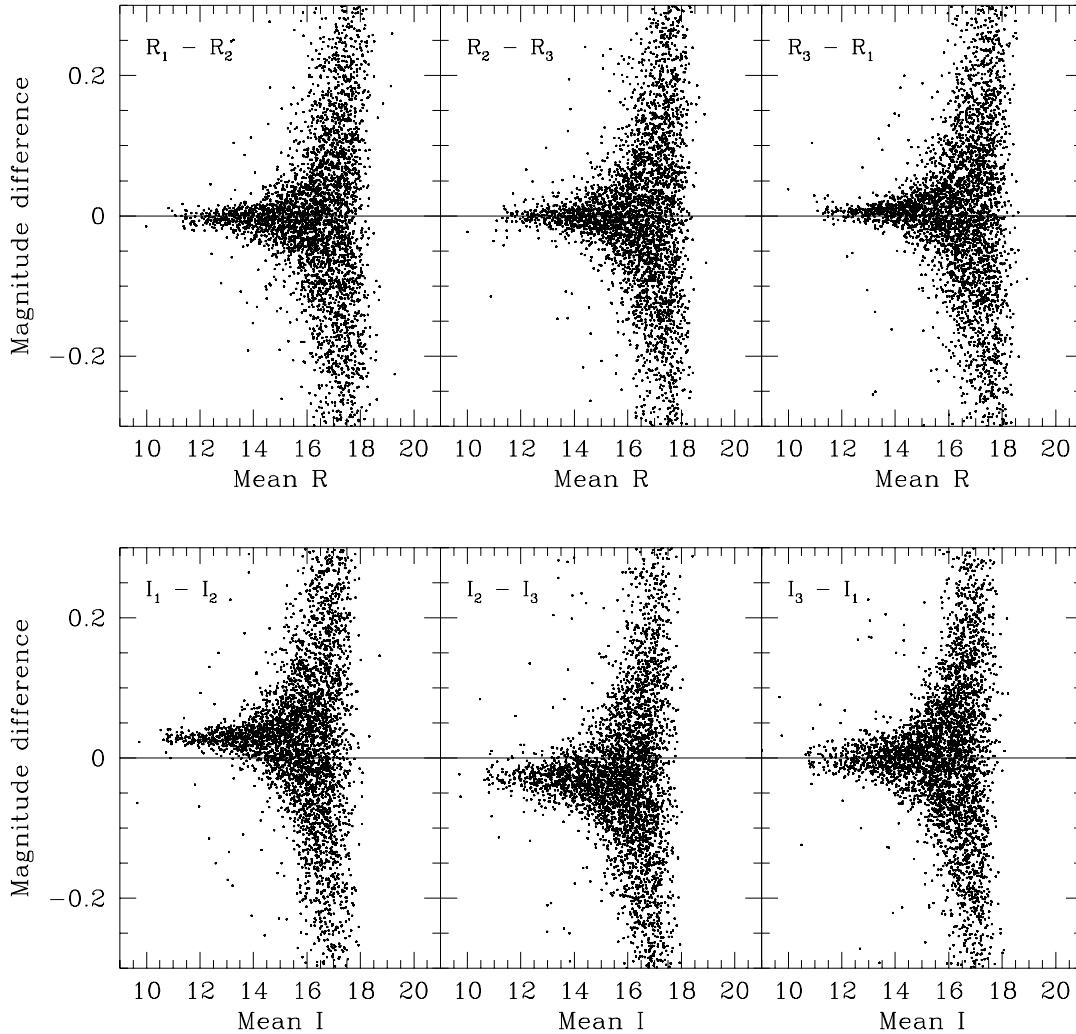
FIG. 3.—Demonstration of normal vs. defective photometry. The plots show the difference of measured photometry from two exposures of the same field as a function of magnitude. Each row shows the three permutations of the difference between two of the three exposures taken per filter. The top row shows an excellent set of exposures, while the bottom demonstrates a case where exposure number 2 generates photometry 0.030 mag fainter than the other two exposures.

should also be small. Thus, our only outstanding concern for these fields is that the extinction might have been non-uniform. The photometric offsets for the opposing edges were similar, so we suspect that the data are of acceptable quality.

In summary, we have obtained *VRI* photometric data for 320,917 stars over 60 degrees² with a typical photometric precision of 0.032 mag in all bands for stars brighter than $R = 16$.

3. SEARCH FOR PMS STARS

3.1. *Technique*

Our goal is to use these photometric data to identify a statistical sample of PMS stars in the λ Ori star-forming region. We have demonstrated in Papers I and II that using spectroscopic data combined with multicolor photometry we can securely identify young association members despite the fact that field stars outnumber the members by factors of several hundred. In this section, we demonstrate that we can use the knowledge gained from our spectroscopic sur-

vey to identify a statistical sample of stars which closely resemble the PMS population (in number, spatial distribution, and photometry) using the photometric data alone. As a proxy for the true PMS population, we will use this sample to study the spatial distribution of young, low-mass stars over the entire λ Ori region and to compute the IMF of the star-forming complex.

Our technique relies on the fact that PMS stars have R versus $R-I$ CMD positions rather different from most field stars. Additionally, we use the information from Papers I and II that the PMS stars lie in a small range of ages at about the same distance. Exploiting these characteristics allows us to maximize PMS stars while minimizing field stars in a photometrically selected sample. We use the R, $R-I$, and $V-R$ measurements of confirmed PMS stars to define photometric boundaries in which the field star contamination will be as low as possible.

3.2. *Calibration*

The first step is to define a region of the CMD that has a high ratio of PMS stars to field stars. We use our spectro-

scopic PMS population from Paper II as a calibration sample, or control group, to define such a region before applying it to the fields where we have no spectroscopic information. Figure 4 shows the location of these spectroscopically identified PMS stars, along with a large population of field stars in the same lines of sight. Using a line at $R = 16$ along with isochrones and mass tracks from the Palla & Stahler (1999) stellar evolution model as boundaries, we can isolate a region in the CMD which has many PMS stars and few field stars. Specifically, we have selected an isochrone at 4 Myr and a mass track at 0.6 $M_\odot$ (both at 450 pc) as optimal boundaries to minimize field contamination.

We further cull field stars from the spectroscopic control sample using the $V-R$ colors. Figure 5 shows all of the field and PMS stars which fulfill the criteria in the R versus $R-I$ domain. For this subsample, the PMS stars form a well-defined locus in the R versus $V-R$ CMD, while the field stars are much more broadly distributed, particularly brighter and redder than the PMS stars. We have chosen a pair of boundaries, shown in the figure, which remove 28% of the field stars at the expense of only 1% of the PMS stars. The resulting $V-R$, $R-I$, and R boundaries yield roughly equal numbers of PMS (179) and field (232) stars.

3.3. Application to Survey

Next we use these photometric boundaries to select candidate PMS stars in survey fields for which we do not have spectroscopic information. Figure 6 shows the spatial distribution of all stars which fall within the photometric criteria defined above. Inset in that figure is an R versus $R-I$ CMD showing those same stars. Comparison with Figure 2 gives a sense of the large extent to which field stars have been removed.
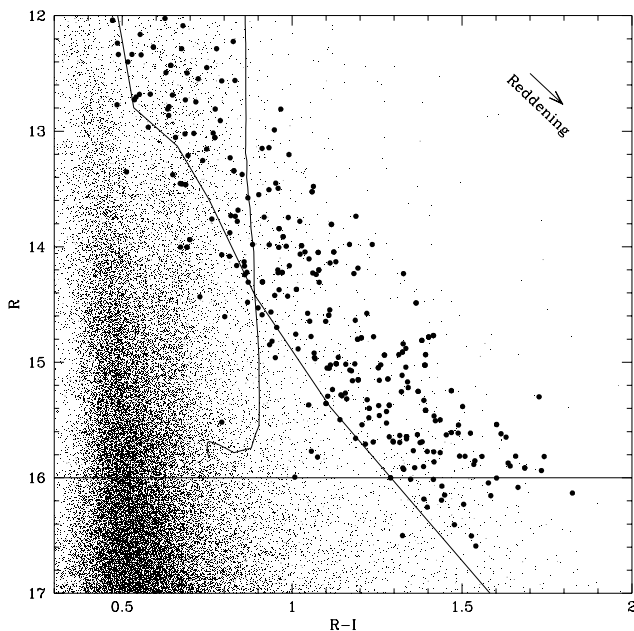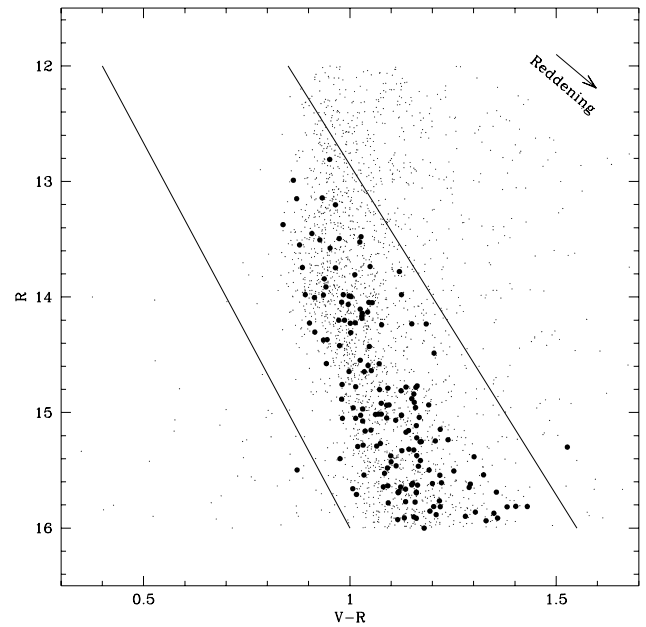

FIG. 5.—R vs. $V-R$ photometric discrimination of PMS stars from the field. The stars shown are those isolated in the upper right of Fig. 4. The lines are the boundaries we derive from this figure for use in isolating PMS stars in the survey fields. The lower line passes through the points $(R-I, R) = (0.4, 12)$ and $(1, 16)$, while the upper line is defined by $(0.85, 12)$ and $(1.55, 16)$.

The most obvious feature of this map is that there are stars everywhere in the region of interest. Based on the analysis of the previous section, more than half of these are field stars, which should have a nearly uniform distribution. Close examination of Figure 6 shows that there are excesses of stars in particular areas. Notably, there is a large excess centered on λ Ori. There is also a distinct clustering of stars near B35. Thus the photometric selection technique is successfully identifying PMS populations in regions where we had previously found enhancements of PMS stars by spectroscopic techniques.

Additionally, the figure appears to show a ring of higher stellar density at the edges of the surveyed region, coinciding with areas where the field star density is shown to be low in Figure 2. However, as we discuss in the next section, these density enhancements may be artifacts caused by reddening in the dark clouds rather than enhancements of PMS stars.

3.4. The Effects of Extinction

When searching for density enhancements in Figure 6, one implicitly assumes that the field star distribution is uniform. However, if a large fraction of the field stars are more distant than the λ Ori association, as indicated by Figure 2, the reddening due to dense gas in the star-forming region can move field stars into our photometric selection region. This change in the morphology of the field CMD can cause an apparent excess in the vicinity of a dusty cloud. That is, the number of non-PMS stars varies as a function of extinction in the star-forming region.

To estimate the magnitude of the extinction, we use the following simple procedure. First, we refer back to Figure 2 of Paper II, which shows the distribution of CO J $= 1 \rightarrow 0$ emission in the star-forming region (Lang & Masheder 1998). The highest contour is 19.2 K km s^{-1}. Lang &

FIG. 4.—R vs. $R-I$ photometric discrimination of PMS stars from the field. The small dots are all the stars in the fields studied spectroscopically. The large dots are the PMS stars found in those same fields. We overlay a line at $R = 16$ along with a 4 Myr isochrone and a 0.6 $M_\odot$ evolution track from the Palla & Stahler (1999) models to indicate boundaries used to isolate the candidate PMS in the upper right.
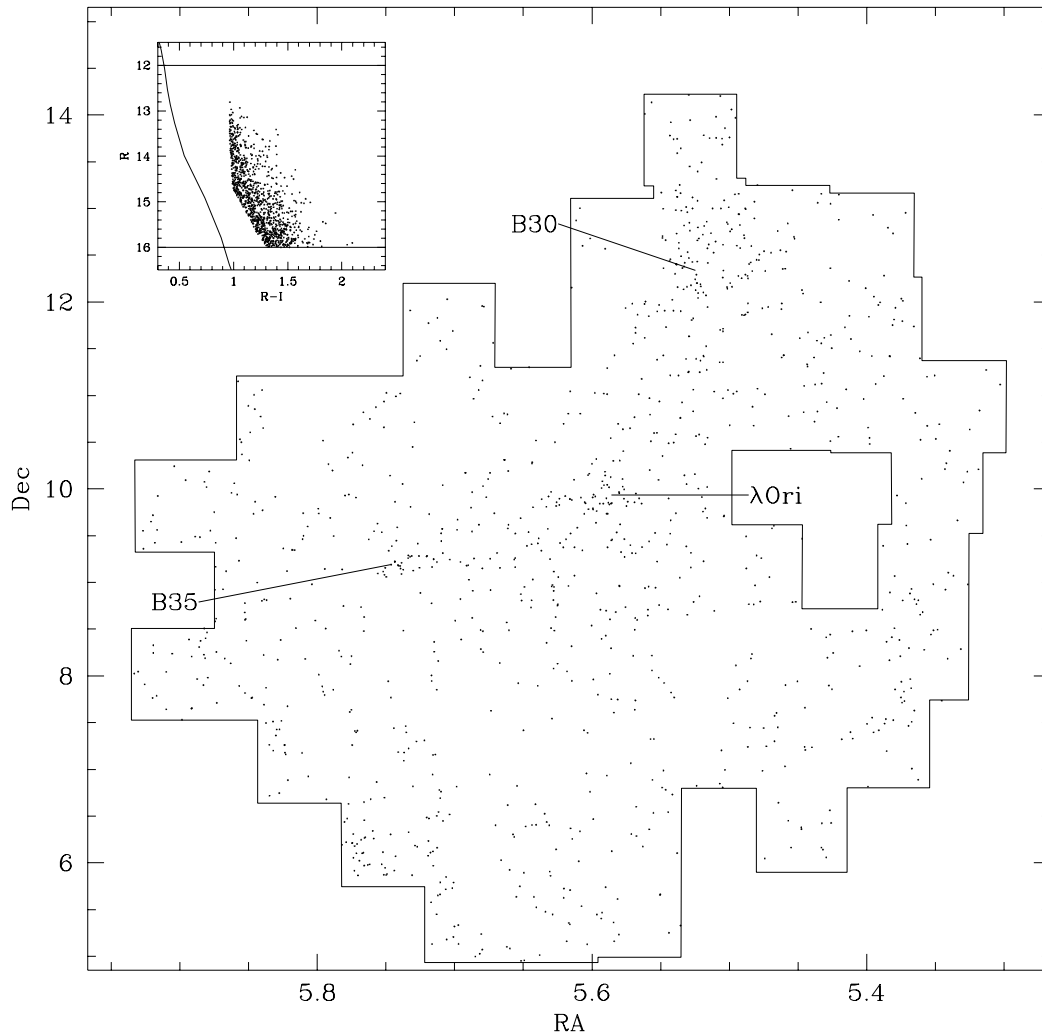
FIG. 6.—Map of all stars selected by the photometric criteria defined in the text (see Figs. 4 and 5). The inset plot shows R vs. $R-I$ for those same stars.

Masheder (1998) quote a conversion from CO brightness temperature to H_2 column density of $(1.06 \pm 0.14) \times 10^{20}$ cm^{-2} (K km s^{-1}) from Digel, Hunter, & Mukherjee (1995) for Orion. Thus the strongest CO emission traces H_2 of column density 2×10^{21} cm^{-2}. Doubling this number to account for the two hydrogen atoms per molecule and using the Bohlin, Savage, & Drake (1978) conversion from hydrogen column density to E_{B-V} color excess of 5.8×10^{21} cm^{-2} mag^{-1}, we find the peak reddening is roughly $E_{B-V} = 0.7$ mag. Using a general-to-selective extinction ratio of $R_V = 3.1$ and the Cardelli, Clayton, & Mathis (1989) extinction law, we find the peak absorption to be on the order of $A_R = 1.6$ mag. If instead we use a higher value of $R_V = 5$, we find $A_R = 2.7$ mag. Certainly, this calculation is only an approximation (for example, it is not clear whether our application of the Bohlin, Savage, & Drake conversion is appropriate for this region). However, it suffices to demonstrate that the dense clouds have nonnegligible extinction, but are not opaque.

Thus, there could be a couple of magnitudes of extinction for background stars where the molecular clouds are densest. The consequence of this is that many of the blue field stars could be reddened into the photometric boundaries we defined above.

To test this hypothesis, we take a field where there is very little molecular gas (as inferred from the CO map) and artificially redden it by a constant extinction, adding some random scatter to simulate varying conditions within the field. Figure 7 shows an example of this test performed on field 151. The top left panel shows the unaltered CMD of that field. To create the CMD in the lower left panel, we added an extinction (A_R) randomly selected from a Gaussian distribution with a mean of 1 mag and a standard deviation of 0.5 mag (discarding any selected extinction below zero). In this example we compute the E_{R-I} reddening from A_R using $R_V = 3.1$. As a comparison, we include in the bottom right panel the CMD of field 65, which should be genuinely reddened as it is projected on the B30 dark cloud where the CO has a high column density.

Note the strong similarity between the bottom two panels of Figure 7 showing one artificially and one physically extincted field. We take this similarity to mean that (1) the on-cloud fields have similar background CMDs to the off-cloud fields, but they have been extincted and reddened; (2) most of the field stars are in the background; and (3) our extinction estimates calculated above are reasonable.

Most importantly, the number of stars in the photometric selection region rises rapidly with increasing extinction.
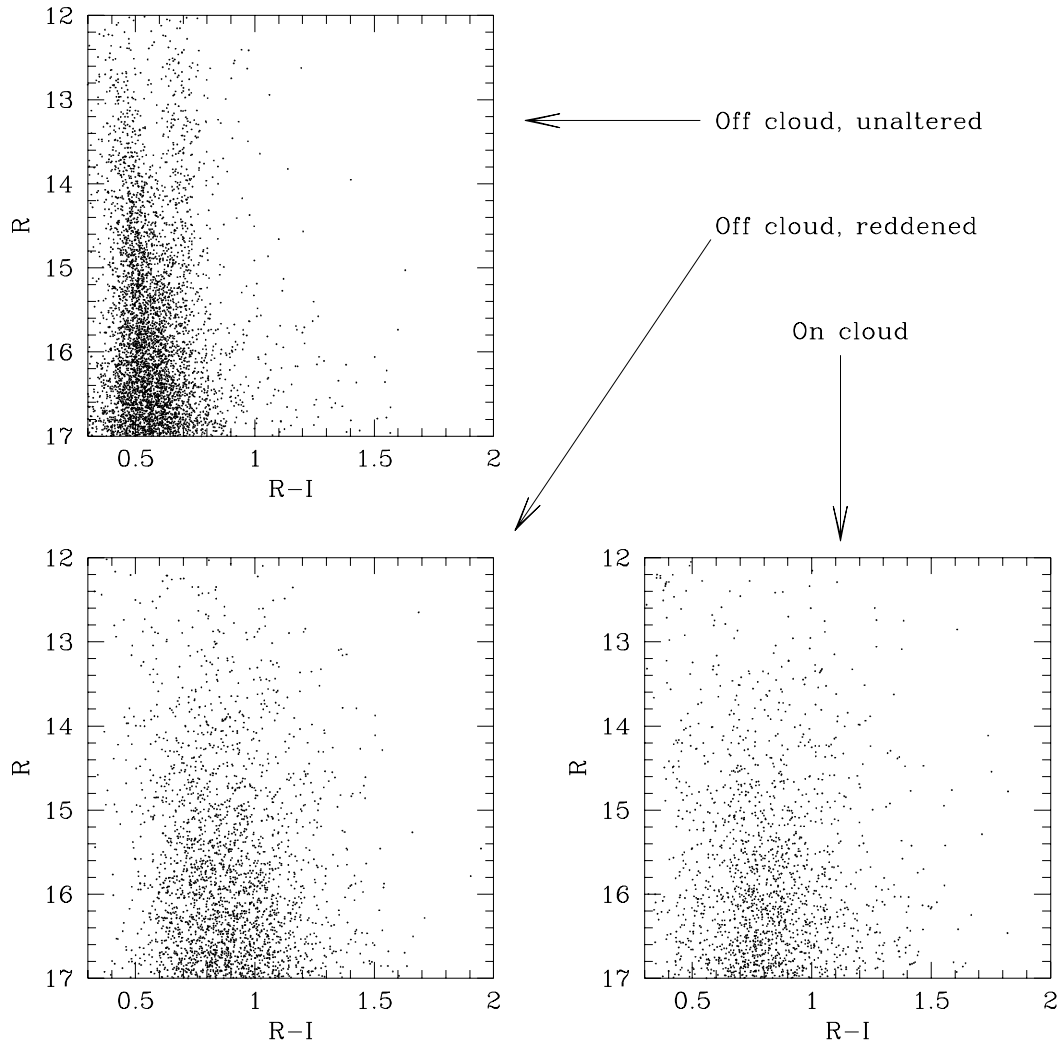
Fig. 7.—Demonstration of the effects of reddening due to the dark clouds. We transform the top left panel to the bottom left panel by adding a normally distributed random amount of reddening with mean and standard deviation of 1 mag and 0.5 mag, respectively. The bottom right panel shows the observed CMD of a field projected on one of the dark clouds as a comparison.

Therefore, we conclude that the apparent excess stellar density projected on the regions of the dark clouds in Figure 6 is likely an artifact of the extinction of background field stars caused by those clouds. This also means that the probability of a bright, red star projected on a dark cloud being a young member of the association is much smaller than one with similar photometry projected on a transparent region.

3.5. *Statistical Removal of Field Stars*

The sample of stars we constructed above contains stars with photometry consistent with PMS members of the association. However, that sample still contains a substantial number of field stars that are photometrically indistinguishable from PMS stars in *VRI*. To study the IMF and spatial distribution of the low-mass λ Ori members, we would like our proxy population not only to contain stars with the correct photometric properties (thus ages and masses), but also to contain the correct number of stars. Ideally, we would simply subtract a constant number of stars from each field to arrive at a statistical estimate of the number of PMS stars in those fields, but unfortunately the field star distribution is not uniform because the background star density decreases

with increasing galactic latitude. Therefore, in this section we describe a technique we have used to determine the number of field stars using the assumption that the unreddened field-star CMD has the same morphology across the entire complex. That is, we assume that the ratio of field stars in one region of the CMD to another region is a constant. We establish this ratio using the spectroscopically studied control fields where we can securely create a sample with only field stars and no PMS stars. Then we use this ratio to subtract field stars in each of the rest of the fields. This yields a measure of the number of PMS stars in each field.

Note that, as described in the last section, the regions with substantial reddening do not have the same CMD morphology as unreddened regions, so this technique does not work well for fields projected on the dark clouds.

In detail, we first identified a region of the CMD that is free of PMS stars (which we call the "PMS-free region" in contrast to the "PMS candidate region" discussed in earlier sections). We defined this by the boundaries $0.5 \leq R-I \leq 0.7$ and $14.5 \leq R \leq 15.5$. Several criteria entered into our selection of this particular region. First, this region is rich with field stars, as seen in Figure 4, for example. The more field stars there are, the less error is

introduced into our calculations by counting noise. Second, this region is faint enough and blue enough that it cannot contain any PMS stars. In fact, this box is almost entirely below the ZAMS at 450 pc, let alone near the PMS stars. Third, it is bright enough that photometric error is negligible.

Totaling over all the control fields except those with poor spectroscopic completeness (as identified in Table 3 of Paper II) and those projected on the densest portions of B30, we find a ratio of 0.033 for the number of field stars[4] in the PMS-candidate zone to the number of stars in the PMS-free region. The counting error associated with this ratio is about 15%.

Next, for each of the fields in our survey we count the number of stars in the PMS-free region and use the above ratio to compute the expected number of field stars in the PMS-candidate region. The difference between this result and the observed number of PMS candidates is an unbiased estimate of the true number of PMS stars.

Finally, for the purpose of creating a map of the PMS stars, we subtract the derived number of field stars from the survey fields. This removal is statistical, since we do not really know which are field stars and which are PMS stars. Thus, for each field we randomly remove a number of stars equal to the expected number of field stars leaving a representative sample of PMS candidates with approximately the same numbers, photometric properties, and spatial distribution of the true PMS population.

The random nature of the removal technique means that the PMS sample is only representative on a field-by-field basis. That is, we find an accurate estimate of the number of stars in each $1°$ field, but we do not know their true positions within that field. Because the fields that are projected on the molecular clouds suffer reddening of the background stars, our technique is invalid there[5] (although it has been applied to all fields for simplicity).

Figure 8 shows the statistical PMS population after subtraction of field stars. Figure 9 shows the same map as Figure 8 rotated into galactic coordinates and overlaid on the CO map of Lang & Masheder (1998). Stellar density enhancements are clearly seen near both λ Ori and B35, confirming similar observations made from Figure 6. *Perhaps more remarkably, much of the region inside the molecular ring is devoid of PMS stars.*

These two figures show a large number of low-mass stars near λ Ori and the neighboring B stars. The stars around λ Ori are present primarily within the $2°$ circle marked on Figure 8. Out to that radius, this distribution is consistent with an r^{-2} density distribution centered on λ Ori. This is reminiscent of the simple kinematic model of the stellar expansion we constructed in Paper I, where we explored (and could not rule out) the possibility that all of the stars around λ Ori had formed in a tight Trapezium-like cluster and then kinematically dispersed when the parent gas was dispersed.

The essential new information from this study is the spatial extent of the population of PMS stars around λ Ori. Even excluding stars in the vicinity of B35, the distribution of PMS stars extends as far as 16 pc from λ Ori. For a one-dimensional velocity dispersion of 2.5 km s^{-1} (as found from radial velocities in Paper I), a typical star would move 2.5–5 pc in 1–2 Myr, while extreme velocity stars might travel as much as 7.5–15 pc. As such it is possible that the spatial extent of the present PMS population around λ Ori derives in large part from ballistic expansion of an initially more concentrated population after a recent gas dispersal event.

Even so, given the substantial fraction of stars found 10–15 pc from λ Ori, it seems unlikely that the distributed population derives entirely from a Trapezium-like cluster around λ Ori. Indeed, as noted in Paper I, it would be odd if the low-mass stars of such a cluster dispersed while the OB stars did not. Thus we conclude that star formation occurred over a distributed region around λ Ori, but quite possibly over a spatial extent more limited than the presently observed spatial distribution of PMS stars.

The edge of this central population of PMS stars abuts on a clump of stars near the B35 cloud. In Figure 9, one can see that this group extends toward λ Ori from the densest portion of the molecular cloud. However, it is somewhat surprising that there appear to be no PMS candidates on the "neck" of the B35 cloud, the elongated portion which connects the dense "head" to the ring. Clearly the star formation rate has differed significantly between the front and the back of this cloud.

Finally, the *lack* of PMS candidates outside of the central population is equally important. Figure 8 shows this dearth most clearly in the region between the two circles. (Again, the surface density enhancements outside the larger circle are not valid representations of the PMS population.) Thus, within the present ring of molecular clouds we find that star formation occurred only within a $2°$-radius circle around λ Ori and near the B35 cloud. We also know from Paper II that star formation has been active in the B30 cloud. It remains to be seen whether any star formation has occurred elsewhere within the molecular ring.

3.6. *The Initial Mass Function*

Using our statistical count of PMS stars to represent the true PMS population, we assess the association IMF in this section. We restrict our sample to $0.4\ M_\odot < M < 0.6\ M_\odot$, which minimizes both incompleteness at the faint end (see § 5.3 of Paper II) and contamination by the field, respectively. In the census completed in Section 3.5, we used an age limit of 4 Myr. However, in Paper II we noted that the onset of star formation occurred about 8 Myr ago. Thus a fair assessment of the IMF should include stars of at least that age. A drawback is that in extending our census to an 8 Myr age limit, the number of field stars increases faster than the number of PMS stars. For stars $0.4\ M_\odot < M < 0.6\ M_\odot$ there are 60% more total stars in the expanded selection region of the CMD, but in the spectroscopic survey we found only a 10% increase in PMS stars in this region (62 PMS stars younger than 8 Myr versus 56 younger than 4 Myr).

Thus we consider two different methods of counting PMS stars to 8 Myr. First, we simply redo the census with an age cutoff of 8 Myr (which involves redoing the field star cali-

---

[4] That is, the number of spectroscopically identified field stars corrected for incompleteness.

[5] Note that just because our technique does not work well on the cloud regions does not mean that there are no PMS stars there. On the contrary, our spectroscopic survey detected substantial numbers of PMS stars projected on the B30 cloud (in the upper right portion of the figure), but these are outnumbered by the reddened field stars masquerading as PMS stars in the figure.
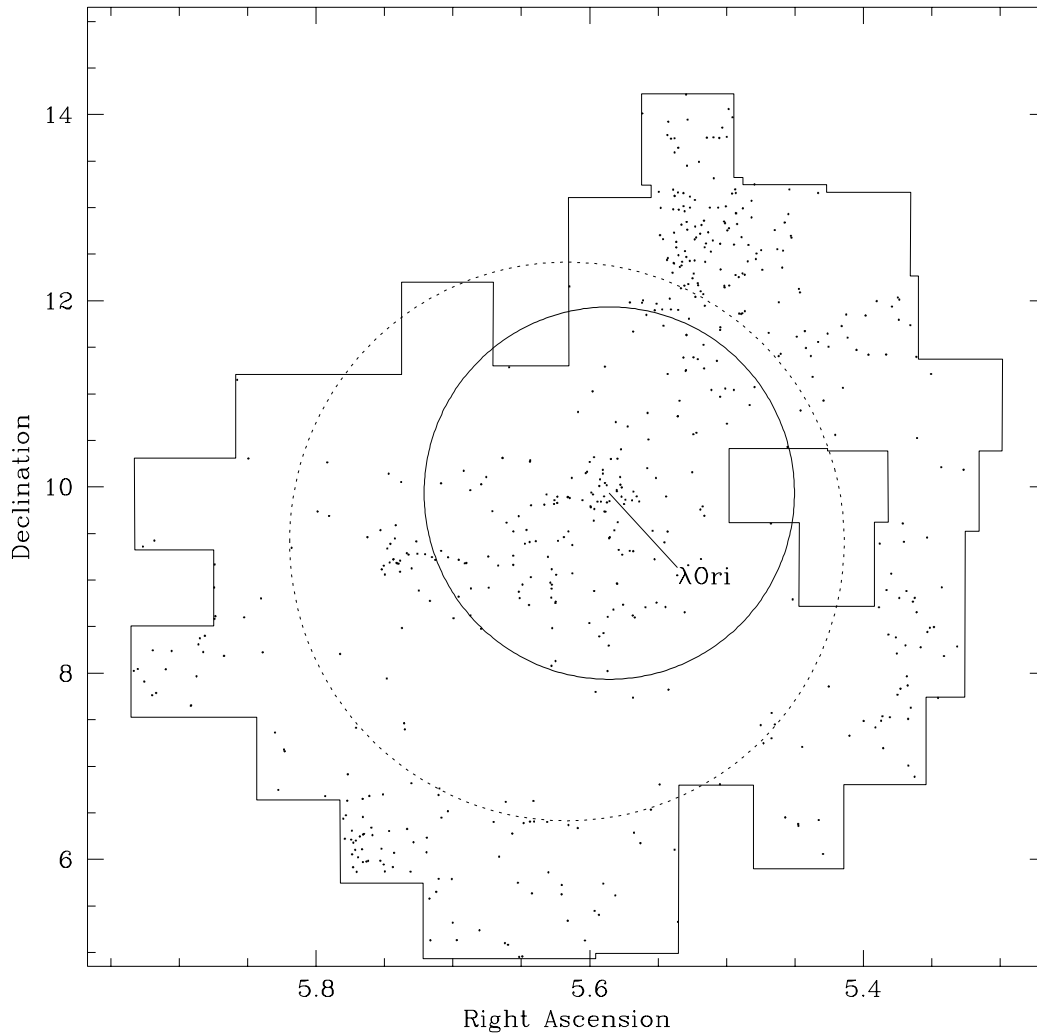
FIG. 8.—Map of PMS candidates with field stars removed statistically. The fields outside the dotted circle are projected on the molecular clouds, so the high surface density of PMS candidates is very likely artificially enhanced by reddening. The dotted circle is centered about 40′ southeast of λ Ori and has a radius of 3°. The solid circle is the 2° radius boundary centered on λ Ori, which we use in Paper II and which is shown in Fig. 2 of Paper II.

bration and rejection of § 3.5). In this case, we count 142 stars with 0.4 $M_\odot < M < 0.6$ $M_\odot$ within the dashed 3° circle on Figure 8. Second, we consider the number of PMS candidates younger than 4 Myr (102) and extrapolate to 8 Myr using the ratio of PMS stars younger than 8 Myr (62) to those younger than 4 Myr (56) found in our spectroscopic survey. This yields an estimate of $(102 \times 62/56) = 113$ PMS stars younger than 8 Myr over the entire star-forming region. This latter computation has the drawback that it implicitly assumes the same star formation history throughout the entire region. Since we do not know which count is more accurate, we will use both the direct count (142 PMS stars) and the extrapolated count (113 PMS stars) in the calculations below. We note that our uncertainty in the calibration of the field star density of 15% yields a 20% uncertainty in the number of PMS candidates.

Using the Miller & Scalo (1979, hereafter MS) field IMF, 142 stars with 0.4 $M_\odot < M < 0.6$ $M_\odot$ predicts 44 OB stars; a count of 113 PMS stars predicts 35 OB stars. In fact, there are only 24 OB stars (as identified in Paper II via the PPM catalog; Roeser & Bastian 1988) in projection within the region of the low-mass star census. Application of the

Monte Carlo test described in Paper I shows that the difference between the observed number and the prediction suggests a difference in the IMFs at the 99.8% confidence level for the direct count and at the 95.8% confidence level for the corrected count. Thus, according to the MS IMF, the low-mass stars are mildly overrepresented in the star-forming region. This overrepresentation is further increased by the fact that there are very likely nonmembers included in the OB census, as discussed in § 3 of Paper II.

We have also tested the field IMF formulation of Kroupa, Tout, & Gilmore (1993), hereafter KTG, which employs three power-law fits to the mass function instead of the log-Gaussian used by MS. The KTG field IMF predicts that, given the direct count of 142 stars between 0.4 and 0.6 $M_\odot$, we should see 20 OB stars. This is more than a factor of 2 lower than the MS prediction above, and it is consistent with the observed number of OB stars. The corrected count of 113 PMS stars predicts 16 OB stars, which is also consistent with the observed number.

Clearly the systematic uncertainties in the field IMF dominate these comparisons. Given that only in the most extreme case can the difference between the field IMF and
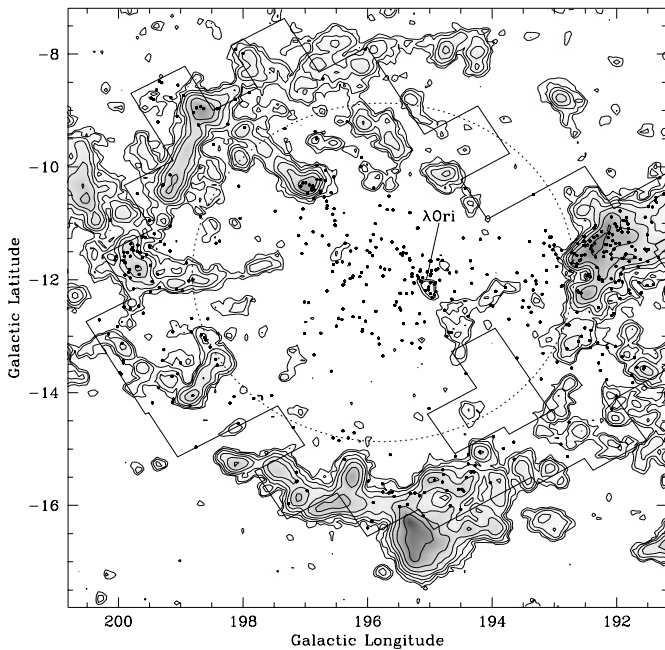
FIG. 9.—Same as Figure 8, rotated and overlaid on the map of Lang & Masheder (1998) in galactic coordinates.

the association IMF be considered significant, we conclude that the global initial mass function in λ Ori is not distinguishable from that in the field.

On the other hand, local variations of the IMF are significant, as reported in Papers I and II: (1) in the central 1° where the OB stars are concentrated, the low-mass stars are *deficient* by a factor of 2; (2) outside of this central region they are *overabundant* by a factor of 3. The spatial distribution of star formation is significantly *mass biased*.

Our count of stars with 0.4 $M_\odot < M < 0.6 \ M_\odot$ plus the 24 OB stars implies a total mass of 450 to 650 $M_\odot$ for stars above 0.1 $M_\odot$ within the molecular ring, depending on the PMS count (113 or 142) and choice of field model (MS or KTG). These mass estimates are a factor of 2 higher than the lower limit on the total mass stated at the end of Paper II, but here we also include more than a factor of 3 more spatial coverage. Compared with the total cloud mass of $4 \times 10^4 \ M_\odot$ calculated by Maddalena & Morris (1987) (including molecular, neutral, and ionized gas), this implies a star formation efficiency of 1%–2%. The molecular cloud mass computed with higher quality CO data by Lang & Masheder (1998) matches that of Maddalena & Morris for the molecular gas ($1 \times 10^4 \ M_\odot$), but they do not include H I or H II mass, so we cannot compute an independent efficiency from their work. One must note that these are mass estimates of the present-day clouds. It is likely that a significant fraction of the natal cloud could be sufficiently heated or dispersed by now that it is not included in the above estimates. But whether the efficiency is 1%–2% or a factor of 2 lower, it is similar to other estimates of global star formation efficiency in molecular clouds (e.g., Myers et al. 1986).

4. INTERPRETATION: THE SUPERNOVA SCENARIO REVISITED

We have created a statistical representation of the entire young stellar population inside of the molecular ring. We have found a large concentration of PMS candidates centered on λ Ori as well a concentration near the B35 dark cloud. More thorough studies of a subset of these stars via WIYN spectroscopy in Papers I and II definitively showed that these populations are composed of genuine young members. In addition, the spectroscopic investigation showed that there are many PMS stars projected on the B30 dark cloud (on the northwest side of the molecular ring), where our purely photometric analysis does not work well. There are no other concentrations of young stars within the molecular ring.

This supports the model proposed by Duerr et al. (1982) that the initial cloud distribution was elongated, extending (at least) from B30 through the center to B35. Thus, the current distribution of young stars is seen as a fossil of the parent molecular cloud, tracing the densest parts of that structure. Our identification of this fossil is only possible because (1) the cloud is mostly dispersed today and (2) the stars have not moved much from their places of birth. This latter point is supported by the kinematic evidence presented in § 3.4 and § 4.4 of Paper I. To recap those arguments, the OB-star proper-motion dispersion and PMS-star radial-velocity dispersion in combination with the present tight spatial concentration of those populations constrain the dynamical timescale to be of order 1 Myr. (See also the note added in proof of this paper.) Eralier than 1 Myr ago, the stars must have been gravitationally bound, presumably by the parent cloud.

But today there are virtually no signs of that parent cloud remaining within the central 2° radius, or 16 pc radius at the 450 pc distance of λ Ori. We have suggested that the cloud was rapidly dispersed by a supernova about 1 Myr ago. We require a supernova instead of more conventional action by OB star winds and radiation primarily to achieve the short timescale: Maddalena & Morris (1987) calculate that more than 3 Myr is needed for the OB stars alone to carve out an H II region of 16 pc radius.

In addition, the dearth of PMS stars younger than 1–2 Myr within 16 pc of λ Ori (discussed in detail in Paper II), despite the abundance of such young stars in the more distant dark clouds B30 and B35, demonstrates that an event centered near λ Ori terminated all low-mass star formation in its vicinity quite recently. The probable mechanism for this termination is the dispersal (again by supernova) of the central cloud from which the stars were forming.

With this evidence as foundation, we construct the following history of the star-forming region. In the course of this discussion, the reader may wish to refer to panels *a*, *b*, *c*, and *d* of Figures 10 and 11, which show schematic representations of this history.

About 8–10 Myr ago, the λ Ori region was composed of a starless, roughly linear string of dense molecular clouds (*a*). The most massive lobes of this cloud chain were the large central core, the progenitors of the present-day B30 and B35 dark clouds, and (south of these) the B223 cloud. The elongated structure of this cloud complex connected to the other linear structures to the northwest and southeast which we see today in the CO map shown in panel *d* of Figure 11.

Over the next few megayears, stars began to form in the densest portions of this cloud chain. At 6 Myr ago, a dozen OB stars formed near λ Ori's present-day position (*b*). The local gas density remained high enough that they could not ionize or disperse more than a small fraction of the gas. Thus, they remained bound to their natal cloud. At the same
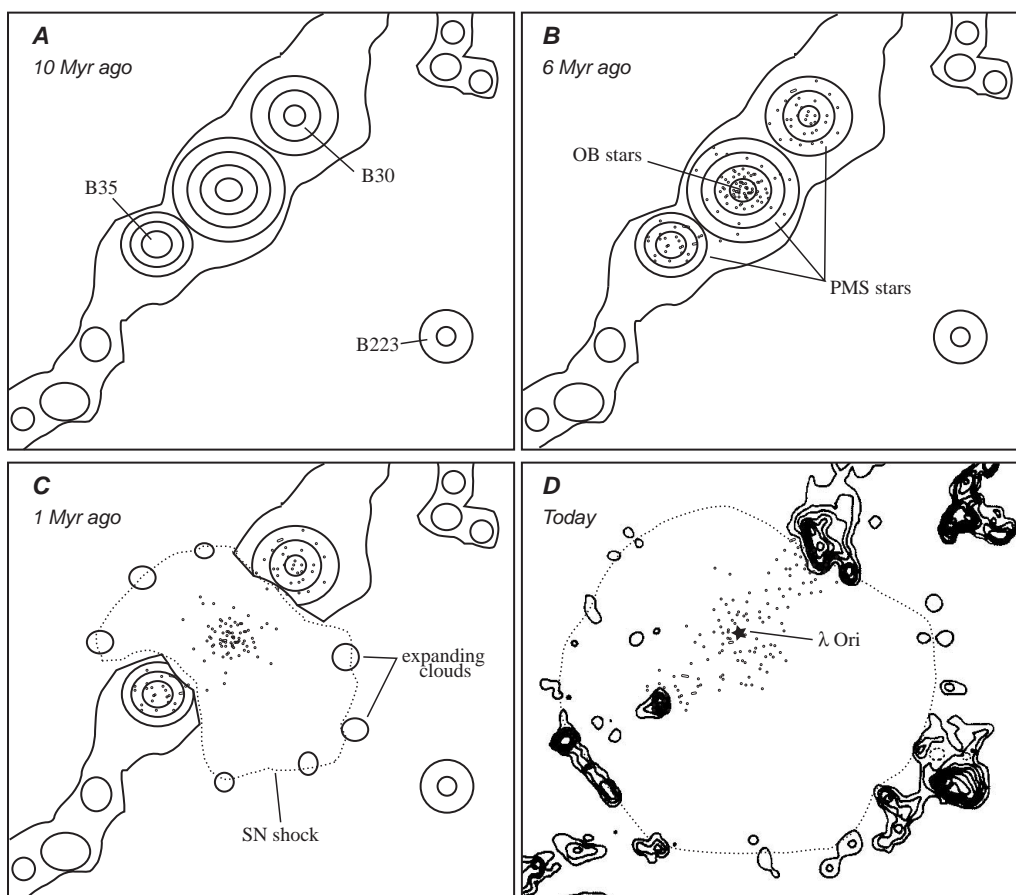
FIG. 10.—Schematic history of the star-forming region showing conditions at 10, 6, and 1 Myr ago, as well as a map of the clouds today with CO contours from Maddalena et al. (1986).

time, the birth rate of low-mass stars increased in all productive areas of the star-forming complex. Many of these were unaffected by the massive stars many parsecs away, but the closest PMS stars passed in close proximity to the OB stars and lost their circumstellar disks to the FUV radiation (Paper I).

Then, shortly before the present day, one of the O stars (perhaps a binary companion of λ Ori itself) became a supernova (c). The supernova blast encountered a nonuniform medium filled with a small H II region forming around the OB stars, dense gas in the immediate vicinity of the OB stars, a few massive clouds about 10–15 parsecs away, and the rest of the volume filled by somewhat lower density molecular gas. The blast quickly dispersed all of the parent core, creating the molecular ring, the large H II region, and the nearby H I structures (Zhang & Green 1991). However, when the shock reached the more distant, massive B30 and B35 clouds, it swept around them. Thus today we see the fossil distribution of young stars within the molecular ring, as well as the remnants of the B30 and B35 clouds within the ionized region (d).

In this scenario we suggest that much of the gas from the parent core has moved as a consequence of the supernova, while the other massive clouds have moved little. This picture differs from the all-expanding model of Maddalena & Morris (1987) and the all-stationary model of Paper II. The Maddalena & Morris model is contradicted because the accelerating gas should have left behind all stars formed therein, whereas we find stars of all ages still projected on B30 and B35 (implying that these clouds have not moved since the oldest stars were born). Also incorrect is our Paper II model of the star-forming region as a single giant cloud with a hole torn from its center, because we have found an annulus inside the CO ring absent of PMS stars. This absence implies that the annulus never had clouds of high enough density to form stars.

Examining Figure 8, one can see the CO ring is not actually centered on λ Ori. We interpret this as evidence of nonuniform gas density: the supernova shock expanded more easily toward (and around) the smaller B35 cloud to the east than toward B30 to the northwest. Over several hundred thousand years, the supernova shock snowplowed the gas outward to where we see the cold ring today. Because the stars have a radial velocity similar to the B30/35 clouds (comparing our data with the Lang & Masheder (1998) and Maddalena et al. (1986) CO data) while the H II gas has a mean velocity several kilometers per second blueward (from the Wisconsin Hα Mapper survey; L. M. Haffner 1998, private communication), it seems the shock must have expanded more readily into lower density gas in the foreground.

Certainly the B30 and B35 clouds have not been totally immune to the shock wave. The inward-facing sides of the clouds have been heavily eroded by the blast. We see a signature of this in the strong density gradients in the molecular clouds facing toward λ Ori, seen in Figure 9. This is a
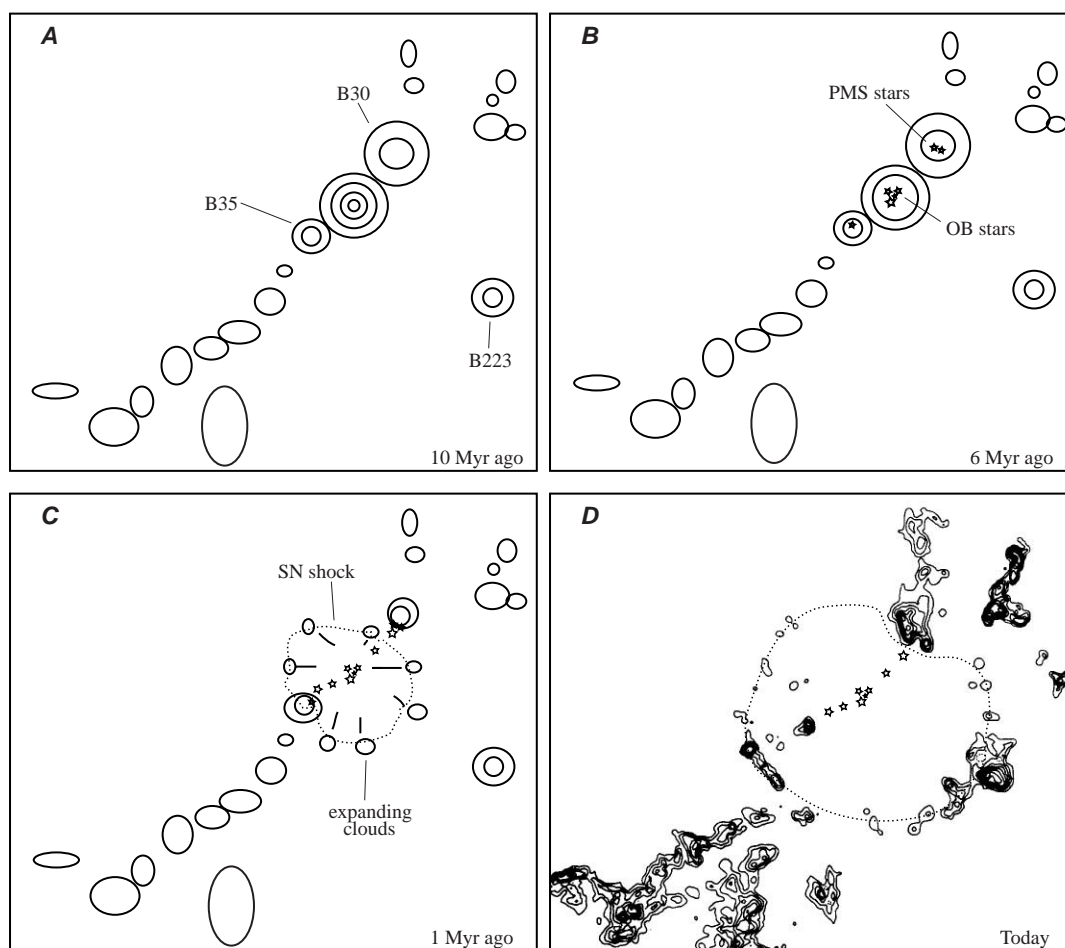
FIG. 11.—Expanded scale version of Fig. 10, showing the environment around the λ Ori region. Again, the CO map is from Maddalena et al. (1986).

consequence of either compression by the supernova (and/ or subsequent OB winds) or by the dispersal of the outer, low-density envelope of the cloud. These same faces show bright rims today (Lada & Black 1976) as they are continuing to be ionized by the remaining OB stars. We also see evidence of the partial destruction of B30 and B35 in the PMS stars that lie slightly in front of the clouds, tracing the former extent of the gas. We reiterate that because the stars in front of the clouds have a wide range of ages matching the age span of the entire association, this enhanced PMS population in front of the clouds is likely a sign of cloud destruction, not cloud acceleration or triggered star formation.

It appears that the supernova had a more devastating effect on B35 than B30, since the former appears to have ceased embedded star formation, while the latter still contains many far-IR sources (Mathieu et al. 1990). All of the PMS candidates near B35 in Figure 9 lie on the side of the cloud facing λ Ori; none lies on the low-surface-density " neck " connecting B35 to the CO ring. We suspect that the B35 cloud will vanish in a few megayears, especially if λ Ori becomes a supernova soon.

There are still enigmas left in the structure of the gas, which are not explained fully by our scenario. First is the history of the B223 dark cloud in the southwest of the star-forming complex. Maddalena & Morris (1987) noted that B223 is blueshifted relative to the rest of the clouds and interpreted this as evidence of expansion of the gas. How-

ever, we have found that all of the PMS stars are at a similar radial velocity to B30 and B35, not at a system velocity intermediate between B30, B35, and B223, as would be expected if all clouds were expanding from a common center. The CO surface density for the B223 cloud is quite high, such that its mass is likely comparable to that of B30. Thus it seems likely that, if B30 was unmoved by the supernova, B223 should be similarly stationary. The radial-velocity difference of B223 suggests that either (1) B223 was not originally connected to the λ Ori progenitor cloud, or (2) B223 is the result of the projection or collision of two clouds: one ejected from the λ Ori vicinity and a denser, unrelated one. This latter scenario is appealing, since the velocity profile presented by Lang & Masheder (1998) shows that B223 spans almost 10 km s^{-1} in radial velocity, which could be a sign of two superposed clouds.

Another puzzle is the presence of a pair of low surface density CO clouds projected very near to λ Ori (Fig. 9). If these clouds are at the same distance as the OB stars, then it is unclear how they could have survived the massive star radiation, let alone a supernova. Instead, we suspect that these thin clouds must be in front of or behind the stellar association. A detailed velocity map with the sensitivity of the Lang & Masheder (1998) survey might help to solve this dilemma.

The scenario we have described includes stars forming near the massive, stationary clouds, but not elsewhere. In

the vicinity of the CO ring, where we cannot photometrically sift the PMS candidates from the field stars, we do not know how many members may exist. Our model of expanding, low-mass cloudlets implies that there should be no old stars in the majority of the ring. A detailed spectroscopic survey in the vicinity of these clouds would answer the question of whether star formation is occurring there or not. We suspect that there could be more stars forming just outside the ring, south of Betelgeuse, where the λ Ori region reaches the "northern filament" identified by Maddalena et al. (1986).

The total mass of stars identified as candidate members is roughly 500 $M_\odot$, which is comparable to an open cluster, but spread over a much larger area (about 30–40 pc diameter). The kinematics indicate that this association will be completely dispersed into the field within a few times 10 Myr. Thus, the λ Ori region may be representative of the process of star formation in moderate-mass molecular clouds.

5. SUMMARY

We have presented photometry of over 300,000 stars in the λ Ori region. Using the spectroscopic survey from Papers I and II to define the photometric characteristics of PMS stars, we culled more than 99.9% of the field stars from our sample. Further statistical field star subtraction then leaves a representative sample of PMS candidates, which has the same spatial distribution and population size as the true PMS stars in the association. This sample presented us with a representative snapshot of the present-day low-mass young stellar population of the star-forming complex. In combination with the more detailed, but spatially limited, results from Papers I and II, this snapshot allowed us to deduce the chronology of the region:

10 Myr ago: A long chain of molecular gas extended from east to west across the present-day star-forming region, including three particularly massive clouds.

6 Myr ago: Stars formed in the most massive clouds, but the onset of formation was not sudden. Instead, the birth rate increased gradually over many million years. Numerous OB stars were born in the central cloud, but were very rare elsewhere.

1 Myr ago: A supernova exploded, shredding the central cloud and thus unbinding the central stellar population. A ring of gas was pushed from the center region.

Today: Star formation continues in the B30 and B35 clouds, but has ceased in the vicinity of the supernova epicenter.

Future: The termination of star birth in B35 is imminent, as is the escape of the OB stars from their central position. All of the stars will disperse into the field over the next 10 Myr or so. The gas may also be further dispersed by subsequent supernovae.

We have found that globally this star-forming region has generated a mass distribution similar to the field population, but the IMF is spatially nonhomogeneous: the center region has favored massive stars, while the periphery has favored low-mass stars.

If the λ Ori region is typical of star formation in medium-mass molecular clouds, then this history tells us that these star/cloud associations are short lived: they terminate themselves from within and are not detectable for more than a few tens of megayears. It is not clear what signals the commencement or acceleration of star birth: in the λ Ori region, stars began to form at a low rate everywhere at about the same time, but most of the stars were formed recently. It would be very enlightening to identify analogues of the λ Ori region at earlier and later stages of evolution to study the turning points of star formation history.

REFERENCES

Bally, J., Sutherland, R. S., Devine, D., & Johnstone, D. 1998, AJ, 116, 293
Bohlin, R. C., Savage, B. D., & Drake, J. F. 1978, ApJ, 224, 132
Cardelli, J. A., Clayton, G. C., & Mathis, J. S. 1989, ApJ, 345, 245
D'Antona, F., & Mazzitelli, I. 1994, ApJS, 90, 467
Digel, S. W., Hunter, S. D., & Mukherjee, R. 1995, ApJ, 441, 270
Dolan, C. J., & Mathieu, R. D. 1999, AJ, 118, 2409 (Paper I)
———. 2001, AJ, 121, 2124 (Paper II)
Duerr, R., Imhoff, C. L., & Lada, C. J. 1982, ApJ, 261, 135
ESA. 1997, The Hipparcos and Tycho Catalogues (ESA SP-1200) (Noordwijk: ESA)
Guillout, P., Sterzik, M. F., Schmitt, J. H. M. M., Motch, C., & Neuhäuser, R. 1998, A&A, 337, 113
Hester, J. J., et al. 1996, AJ, 111, 2349
Hillenbrand, L. A. 1997, AJ, 113, 1733
Kroupa, P., Tout, C. A., & Gilmore, G. 1993, MNRAS, 262, 545 (KTG)
Lada, C. J., & Black, J. H. 1976, ApJ, 203, L75
Landolt, A. U. 1992, AJ, 104, 340
Lang, W. J., & Masheder, M. R. W. 1998, Publ. Astron. Soc. Australia, 15, 70
Maddalena, R. J., & Morris, M. 1987, ApJ, 323, 179
Maddalena, R. J., Moscowitz, J., Thaddeus, P., & Morris, M. 1986, ApJ, 303, 375
Mathieu, R. D., Margulis, M., Sofia, U. J., & Marschall, L. A. 1990, unpublished
Miller, G. E., & Scalo, J. M. 1979, ApJS, 41, 513 (MS)
Monet, D., et al. 1996, USNO-A1.0 (Washington: US Nav. Obs.)
Myers, P. C., Dame, T. M., Thaddeus, P., Cohen, R. S., Silverberg, R. F., Dwek, E., & Hauser, M. G. 1986, ApJ, 301, 398
Palla, F., & Stahler, S. W. 1999, ApJ, 525, 772
Preibisch, T., & Zinnecker, H. 1999, AJ, 117, 2381
Roeser S., & Bastian, U. 1988, A&AS, 74, 449
Shu, F. H., & Lizano, S. 1988, in Interstellar Matter, ed. J. M. Moran & P. T. P. Ho (New York: Gordon & Breach), 65
Sterzik, M. F., Alcalá, J. M., Neuhäuser, R., & Schmitt, J. H. M. M. 1995, A&A, 297, 418
Tian, K. P., van Leeuwen, F., Zhao, J. L., & Su, C. G. 1996, A&AS, 118, 503
Walter, F. M., Vrba, F. J., Mathieu, R. D., Brown, A., & Myers, P. C. 1994, AJ, 107, 692
Zhang, C. Y., & Green, D. A. 1991, AJ, 101, 1006

Note added in proof.—In Paper I of this series, we argued that the expansion age of the OB-star system was much smaller than the stellar evolutionary age. This arguement was based on *Hipparcos* proper-motion measurements for five of the OB stars.

Regrettably, our analysis of the proper motions was done without removing the solar reflex contribution with is not negligible. As such, the trajectories of the stars relative to the molecular ring over 3 Myr shown in Figure 13 of Paper 1 were not correct. The trajectories properly corrected to the center of motion of the five stars still imply that, if their motions have been undisturbed since birth, 6 Myr ago HD 36881 and HD 37035 would have been formed near the present location of the molecu-

lar ring and the motions of all five stars since birth have been such as to form a tight cluster from a widely dispersed group of stars. We still consider this scenario to be implausible.

Equally importantly, the derived two-dimensional velocity dispersion of 3.5 km s^{-1} is unchanged. As noted in Paper I this dispersion implies a one dimensional velocity dispersion comparable to the radial velocity dispersion of 2.2 km s^{-1} measured for the nearby low-mass pre–main-sequence stars. The present projected radius enclosing the 11 OB stars in the center of the star-forming region is 3 pc. As such, the expansion age of the OB-star system is of order 1 Myr. Thus the essential conclusion that the dynamical age of the OB-star system is much less than the stellar evolutionary age of order 6 Myr remains unchanged.

We also note here that given this two-dimensional velocity dispersion and adopting a half-mass radius of 1 pc, the mass required to gravitationally bind the OB stars is of order 5000 M. The total stellar mass in the vicinity of the OB stars in a couple hundred M. Thus the OB-star system must presently be in very nearly free expansion.

These arguments strongly suggest that the OB-star system, and likely the low-mass stellar system associated with it, were gravitationally bound as recently as I Myr ago, as argued in Paper I. We suggest that the OB stellar system was initially bound by the parent gas and likely was in a much more compact configuration at the time.